ELSEVIER

Chemical Geology 180 (2001) 19–32

CHEMICAL GEOLOGY
INCLUDING
ISOTOPE GEOSCIENCE

www.elsevier.com/locate/chemgeo

Microbial response to surface microtopography: the role of metabolism in localized mineral dissolution

Katrina J. Edwards [a,*], Andrew D. Rutenberg [b]

[a] *Department of Marine Chemistry and Geochemistry, Woods Hole Oceanographic Institution, McLean Lab, MS#8, Woods Hole, MA 02543, USA*

[b] *Department of Physics, Dalhousie University, Halifax, NS, Canada B3H 3J5*

Abstract

We examine the role of microtopographical surface features on sulfide minerals in localizing and aligning bacterial adhesion. Experimental data shows strong correlation between bacterial cell alignment and principal crystallographic axes of pyrite (⟨100⟩ and ⟨110⟩). While bacteria often adhere to visible surface imperfections such as scratches, in many cases no associated surface features are visible. Additionally, the size of the surface imperfection does not unambiguously determine its effect in localizing and aligning bacterial cells. We theoretically model bacterial adhesion. We find that the depth of a surface feature such as a scratch is less important than its cross-sectional shape. Surface features that conform to the bacterial shape can strongly alter local bacterial adhesion energies, even with heights of only 10 nm. Hence, small local surface alterations due to bacterial metabolism could strongly affect local adhesion parameters, and may account for the observed bacterial distributions on mineral surfaces.

Keywords: Bacteria; Mineral surfaces; Attachment; Pyrite; Dissolution; Sulfur

1. Introduction

Microorganisms mediate many Earth processes, such as mineral dissolution and precipitation, which impacts geochemical cycling of elements at all length and time scales. At Earth's surface and in the subsurface, some microbial cells are free living, but most exist attached to surfaces (Hazen et al., 1991). Since the bacteria affect mineral surface chemistry at their local attachment sites (Silverman and Ehrlich, 1964), these sites are relevant to overall mineral dissolution. Indeed, it has been shown that the degree of bacterial colonization correlates well with surface etching of environmental samples (Bennett and Hiebert, 1992; Bennett et al., 1996; Hiebert and Bennett, 1992). However, the distribution of microorganisms in the environment is heterogeneous, and most of what controls the observed variability is poorly understood.

Most existing treatments of bacterial adhesion have focused on the variability due to different bacteria or due to different mineral substrates. These interactions are characterized either thermodynamically from surface and solution chemistry (Devasia et al., 1993; Marshall et al., 1971; van Loosdrecht et al., 1990a,b; Scholl et al., 1990a; Absolom et al., 1983; Yee et al., 1999), or by spatial interactions such as DLVO theory and its extensions (see review by Hermansson, 1999). While these studies provide important constraints on cell–surface interactions,

* Corresponding author. Tel.: +1-508-289-3620; fax: +1-508-457-2183.

E-mail address: kedwards@whoi.edu (K.J. Edwards).

0009-2541/01/$ - see front matter
PII: S0009-2541(01)00303-5

the role of mineral microtopography has been relatively neglected.

In this paper, we focus on how microtopography could control cell attachment to mineral surfaces. We present theoretical calculations and experimental studies that indicate that microtopography—as induced by the crystallographic orientation of the mineral surface, by surface preparation techniques, and by bacterial metabolism—can bias bacterial alignment on mineral surfaces.

2. Adhesion mechanisms

Intermolecular forces between cells and mineral surfaces can be approximated with colloidal DLVO theories (van Loosdrecht et al., 1989; Hermansson, 1999) that estimate the Gibbs-free energy as a function of the distance between the surfaces. At the medium ionic strengths relevant to many natural systems, the sum of attractive van der Waals forces and repulsive electrostatic interactions often leads to a shallow "secondary minimum" associated with reversible bacterial attachment, separated by a potential barrier from an infinitely deep "primary minimum" at very short separations. In practice, substrate roughness and bacterial surface features such as lipopolysaccharides can impose an additional strong short-range steric repulsion that masks the primary minimum but leaves the secondary reversible minimum. Irreversible attachment, i.e. attachment energies so large that thermal fluctuations are insufficient for detachment, can then be achieved through the bacterial production of extracellular polysaccharides, pili, fibrils, and other bridging appendages between the bacterial and mineral surfaces.

One simplification used in a purely physicochemical approach to cell attachment arises from treating the bacterial and mineral surfaces as hard and atomically flat with isotropic surface properties. To some extent, this is a justified approximation, since laboratory studies have verified that average surface properties do strongly affect attachment rates (Absolom et al., 1983; Edwards et al., 1998; Scholl et al., 1990b). However, there is evidence that micro-scale variations in surface properties also affect microbial attachment. These variations might be included in a structural energy term within a DLVO theory, which could then be used to explain variations of adhesion densities. However, it is unwieldy to treat bacterial alignment with such terms. Instead, we will reconcile the phenomenology with a simple and generic attractive interaction in combination with explicit substrate surface features. We briefly address structural energies again at the end.

3. Experimental microtopographical effects

It is provocative to examine several examples of microbial alignment and localization on sulfide surfaces. We attempt to qualitatively reconcile these examples with an attractive reversible interaction between the microbial and mineral surfaces. To do this, we assume that the effective range of the interaction is much smaller than the scale of bacteria, i.e. much less than a micron. This is the case for DLVO theories mentioned in the previous section where the secondary minimum is typically at a few nanometers of separation (van Loosdrecht et al., 1989). We also assume that irreversible attachment, if it occurs prior to sample imaging, does not significantly change the initial alignment of reversibly bound bacteria. We also approximate the substrate–bacterial interaction as independent of surface orientation. This will not always be appropriate, since locally exposed regions of high surface energy can affect attachment of bacteria at surface imperfections (Banfield and Hamers, 1996). If surface-orientation-dependent interaction energies are accurately measured, they can be straightforwardly incorporated.

Cells can preferentially attach to visible naturally occurring or sample preparation-induced micro-scale surface features such as scratches, pits, and grooves. This is illustrated in Fig. 1 with dual images of a metal sulfide surface. Linear scratches produced from polishing the surface can be readily detected on this surface in reflected light (right). The linear scratches clearly coincide with high densities of oriented cells (left) after reaction with a bacterial cell culture.

Cells will attach in such a manner as to maximize cell–surface contact with the mineral surface, i.e. oriented along rather than across a surface scratch such as in Fig. 1. However, there would also need to be a significant energy difference associated with surface microtopography, compared to the thermal

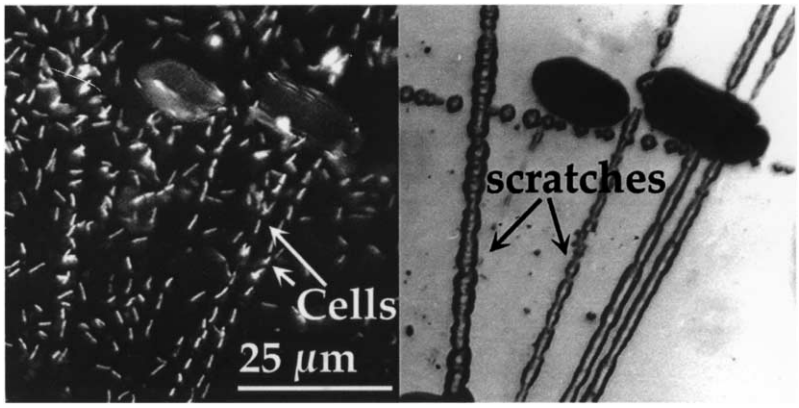

Fig. 1. Bacterial cells preferentially adhering to polishing scratches on a pyrite surface. Left: cells are stained with DAPI (4′, 6-diamidino-2-phenylindole) and viewed in UV. Right: reflected light image of same surface as left, showing linear scratches that were generated with polishing grit. Scale bar on left applies to both images (modified after Edwards et al., 1998).

energy k_BT, for cell alignment to be significantly biased. Surface scratches and other surface features do not always localize or align cell attachment. This is illustrated by the SEM image of another sulfide mineral surface shown in Fig. 2, where scratches in region 1 that are finer than those shown in Fig. 1 do not localize cell attachment. While our qualitative approach is consistent with apparent differences in cell alignment, a quantitative approach (see below) allows specific predictions to be made. We also consider whether scratch shape can account for exceptions such as the cell in region 2 that is clearly aligned along a finer-scale scratch relative to the scratch region 1, or whether they must simply be regarded as statistical fluctuations.

Furthermore, many of the bacteria in Fig. 2 align with no visible surface features, though parallel to unassociated surface dissolution features, shown in the high-resolution inset. Such dissolution pits align with principal symmetry directions (shown with arrows in the inset) to minimize surface-free energy. Indeed, while bacterial alignment parallel to the crystallographic axes of various minerals is often observed, the alignment generally bears no specific relationship to surface features detectable by light or electron microscopy (Edwards et al., 1998, 1999, 2000a). Fig. 3 shows images of cells attached to three different metal sulfide minerals; the inset Fourier transforms indicate that in each case cells preferentially align in two clear directions. On the

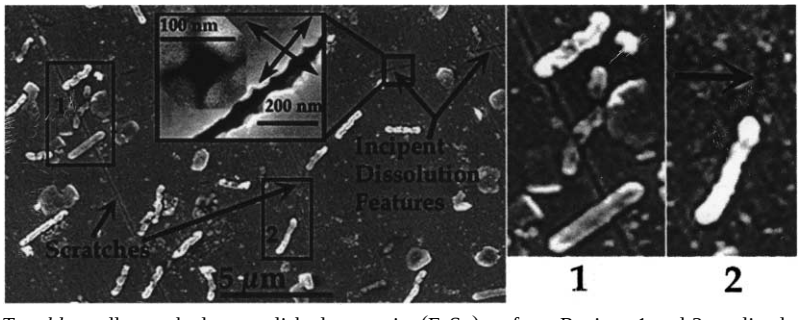

Fig. 2. SEM images of *T. caldus* cells attached to a polished marcasite (FeS_2) surface. Regions 1 and 2, outlined on the left, are shown at higher resolution on the right. Region 1 shows cells aligned nearly perpendicular to a fine-scale polishing scratch. Region 2 shows a cell aligned along a polishing scratch that is finer scale than the scratch in region 1. The inset on the left is a high-resolution image of a developing dissolution pit illustrating the directions that pit edges propagated (shown with arrows; modified after Edwards et al., 2000a).

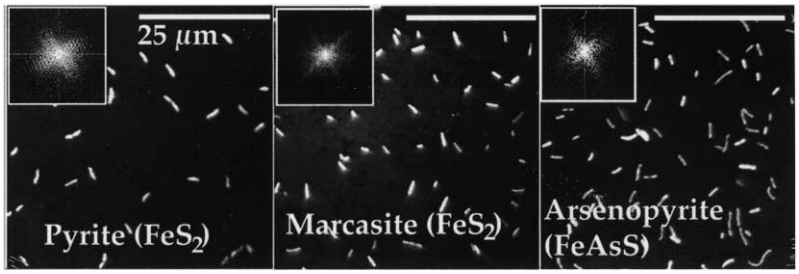

Fig. 3. Bacterial cells attached (not removed after washes) to metal sulfide minerals. Cells are stained with DAPI and viewed in UV. Inset shows Fourier transforms for each respective region, illustrating the directions of preferential cell alignment. For pyrite, these directions coincided with ⟨110⟩. Scale is the same for all images (modified after Edwards et al., 2000a).

pyrite surface, cells shown here are aligned parallel to ⟨110⟩. Cells attached to pyrite surfaces have also been found to align parallel to ⟨100⟩ (Edwards et al., 1998, 1999). On pyrite, ⟨100⟩ and ⟨110⟩ are the directions in which oxidation fronts propagate (Eggleston, 1997; Eggleston et al., 1996) and that dissolution pit edges align with (Edwards et al., 1998, 1999). In the case of arsenopyrite and marcasite, the crystallographic axes were not determined but in each, cell alignment coincided with dissolution pit edge directions (slightly oblique to 90° in both), and so is inferred to coincide with principal crystallographic axes. The cause of this apparently pervasive alignment of bacteria attached to sulfide minerals, but unassociated with visible surface features, is a compelling open question.

4. Quantitative model for reversible bacterial adhesion

The total adhesion energy of the bacterium with the substrate will depend on the details of the interaction potential, the surface geometry, and the bacterial shape. In principle, the bacterium may deform to increase the amount of surface close to the substrate and thereby increase the binding energy. However, any deformation costs elastic energy, which offsets the enhanced surface interaction. The effects of bacterial elasticity and mineral microtopography will be significant only if they affect the total binding energy by a significant amount compared to the thermal energy $k_B T$.

We limit ourselves to discussing adhesion of *Thiobacillus caldus* (Hallberg and Lindström, 1994), a Gram-negative acidophile bacterium that derives energy from oxidizing reduced sulfur compounds such as those that precipitate on sulfide surfaces during oxidative dissolution (McGuire et al., in press). While the elastic properties of *T. caldus* are subject to uncertainty, no extracellular coat is visible in electron micrographs (e.g., see Fig. 2). In contrast, LPS known to be present surrounding other acidophiles, for example *T. ferrooxidans*, is generally readily imaged with a SEM (Edwards et al., 2001). We conclude that *T. caldus* lacks a significant LPS coat. We therefore model *T. caldus* as a simple, homogeneously elastic thin-walled cylinder of length $L = 1.5$ μm and radius $R = 0.32$ μm (Edwards et al., 2000a). We use a Young's modulus of $E = 5.0 \times 10^7$ N/m^2 (Thwaites and Surana, 1991; Yao et al., 1999), a Poisson's ratio of $\upsilon = 0.25$, a wall thickness of $t = 30$ nm (Yao et al., 1999), and a turgor pressure of $P = 3.0 \times 10^5$ N/m^2 (Pinette and Koch, 1987; Beveridge, 1988; Overmann et al., 1991). These parameters are typical for a Gram-negative bacterium such as *T. caldus*. We do not constrain the bacterial volume, since the bacterial membrane is permeable to water (Beveridge, 1999), but we start with a flaccid bacterial radius of $R = 0.25$ μm and achieve the final radius due to turgor pressure.

The specific interaction potential between *T. caldus* and a mineral substrate should, in principle, be determined empirically. Unfortunately, existing methods are not yet consistent. Atomic force microscopy (AFM) studies of *Escherichia coli* adhesion (e.g., Ong et al., 1999; Lower et al., 2000) adhere bacteria to an AFM tip and then probe various surfaces. However, it is unknown exactly how

many bacteria are effectively interacting with the substrate or whether the binding agent between the AFM tip and the bacteria affects the interaction between bacteria and substrate. Strong hysteresis effects (Lower et al., 2000) can also be seen, indicating irreversible adhesion may take place with the substrate. Typical adhesion forces on the order of 1 nN per bacterium are observed, acting at distances on the order of 10 nm. The corresponding binding energy per bacterium, several thousand k_BT, is enormous and would preclude any spontaneous detachment or statistical fluctuations. In contrast, our qualitative observations indicate that detachment does occur and alignment is never perfect. However, we take the interaction range as approximately correct. Flow experiments achieve desorption with forces as low as 10^{-14} N with most detachment occurring by 10^{-12} N (Morisaki, 1991). Assuming a similar range of interaction, this results in a binding energy of 1–100 k_BT. This is consistent with DLVO theories (Meinders et al., 1995). We approximate the interaction by an exponential with an interaction strength of $V_0 = 27\ k_BT/\mu m^2$, corresponding to a total binding energy of $\sim 5\ k_BT$ (van Loosdrecht et al., 1989), and allow it to exponentially decay away from the surface with decay length $\eta = 15$ nm (Ong et al., 1999). This exponential interaction is integrated over the substrate below the bacterium to determine the binding energy. Our results on elastic deformation are relatively insensitive to these parameters. This minimal interaction is simple to work with and is consistent with existing measurements. We do not use DLVO interactions, since the contributing terms are currently poorly constrained by experiments. However, our results will be qualitatively unchanged for other potentials with similar strength and range.

To investigate elastic deformations of the bacterium while it interacted with substrate features, we built a finite-element elastic model of the bacterium with bending modulus $k_b = Et^3/[12(1-\nu^2)]$ and stretching modulus $k_a = E\nu t/[(1+\nu)(1-2\nu)]$ (Landau and Lifshitz, 1986). We relaxed 1000 points along the bacterial perimeter to minimize the sum of the elastic and interaction energies. We found in all cases that the elastic deformation of the bacterium due to surface interaction is minimal, and a circular cross-section is maintained throughout. This is illustrated in Fig. 4, where the binding energy with a flat surface is proportional to the interaction strength, up to enormous surface interactions of 100 000 $k_BT/\mu m^2$, where the constant of proportionality is the effective bacterial-binding area of 0.3 μm^2—given by the patch that is within the interaction range η of the substrate, of width $d = 2(2\eta R)^{1/2} \approx 0.2$ μm and of length L.

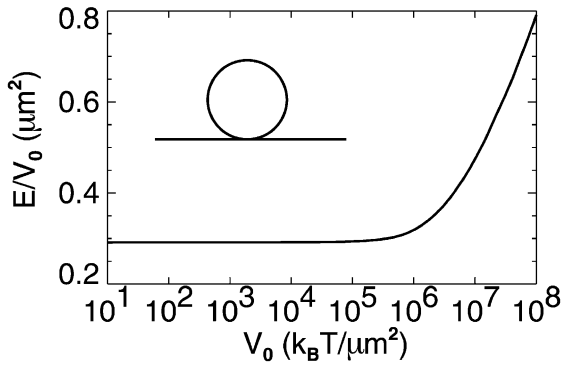

Fig. 4. Ratio of the binding strength E of a bacterium on a flat surface (as shown) to the interaction V_0 as a function of the surface interaction. The constancy of the ratio up to huge interactions indicates that no significant deformation of the bacterium occurs for physically reasonable binding strengths. As a result, the binding strength will be linearly dependent on the interaction range, as long as the range is much less than the bacterial radius R.

In summary, for an enormous range of interaction potentials, we find that the elastic effects are unimportant and that the bacterium behaves like a rigid object. Consequently, from the unattached bacterial and surface geometry alone, we can quantitatively model the observed anisotropies and binding specificities with respect to simple surface features. We will consider bacteria in contact with the substrate, and examine how the binding energies depend on bacterial alignment.

5. Binding calculations

Consider a bacterium lying along a scratch or groove in the substrate. Very small scratches, smaller than the range of the surface interaction, should have little effect on the local interaction and the overall binding strength. Scratches that are large enough to decrease binding, but too small for the bacterium to fit them, will reduce the contact area of the bac-

terium aligned parallel to them. Grooves that are on order of the bacterial size will increase the contact area and hence binding potential, while very wide grooves that are much larger than bacterial dimensions should approach the binding potential of a flat surface. We have calculated these binding energies for a "V"-shaped groove (with faces at a 45° slope) and a "U"-shaped groove (with circular cross-section) as a function of their radius, see Fig. 5. To do this, we have integrated the attractive exponential interaction,

$$V(r) = V_0 \exp(-r/h) \quad (1)$$

over the substrate below the bacterium where r is the closest distance to the bacterium (as before). The binding strength is reduced by the small grooves, but increased when the groove exceeds a critical radius that is close to the bacterial size. The semi-circular "U" groove in particular, can dramatically enhance the binding strength of bacteria with the same or slightly smaller radius. The cross-sectional shape of the groove has a large effect on binding potential,

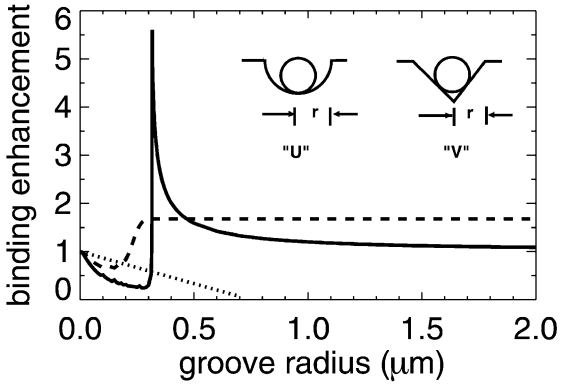

Fig. 5. The enhancement factor over a flat surface as a function of groove radius R for "U"-shaped and "V"-shaped grooves (solid and dashed, respectively). The binding strength is the enhancement factor times the binding strength on a flat substrate (see Fig. 4). The bacterial radius is 0.32 μm, which coincides with the discontinuous increase in binding strength at that radius for "U"-shaped grooves. No such discontinuous increase is seen with "V"-shaped grooves, though both exhibit a reduced binding below the bacterial radius and enhanced binding above. Also shown is the binding strength for bacteria aligned perpendicular to the groove (dotted), which applies to either groove profile. Bacteria will preferentially align perpendicular to the groove if the groove radius is much less than the bacterial radius.

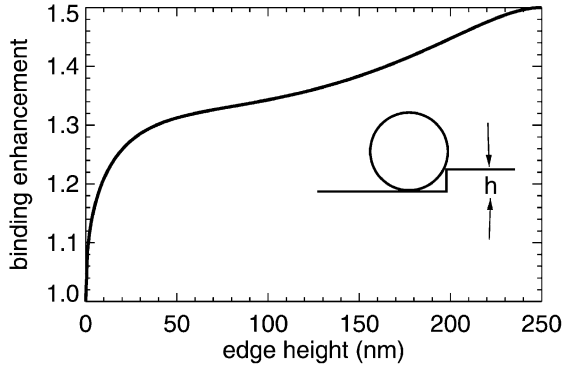

Fig. 6. The enhancement factor of the binding strength for a step-edge resting against the bacterium (as shown) plotted against the step-edge height h. The binding strength is the enhancement factor times the binding strength on a flat substrate (see Fig. 4).

and must be known for the interaction to be fully understood.

For cells oriented perpendicular to an isolated groove (for either "U" or "V" grooves, solid and dashed, respectively), the binding energy will only be reduced by the missing binding over the groove (as shown in the linear decrease with groove width in Fig. 5, dotted line), so that the binding energy for perpendicular alignment is larger than for longitudinal alignment along small grooves—in qualitative agreement with experimental observations where bacteria seem to align perpendicular to small grooves. Bacteria at oblique angles to the groove are not expected compared to either perpendicular or aligned orientations, since excess binding area is lost in the former and the bacteria cannot rest within the groove in the latter.

While bacterial alignment is therefore consistent with the visible microtopography of a mineral surface, the alignment mechanism with respect to the mineral's crystallographic axes in the absence of visible surface features remains speculative until nanoscale features can be characterized during binding studies. One type of small surface feature can be ruled out. For a vicinal surface with a relatively small 1° miscut, compared to a symmetry plane, we expect steps of height ≈ 1 nm every 60 nm. For such a periodically corrugated surface, we obtain a quantitative estimate of the contribution of stretching elasticity and turgor pressure using an analytical

treatment for exponential interactions that is valid for small deformations (Swain and Andelman, 1999). With an effective surface tension due to the competition between stretching and turgor pressure of $\sigma = PR$ (Boal, 1997), we find that the distance over which the bacterium will bend to conform to the substrate is $\xi_\sigma = (\sigma\eta/V_0)^{1/2} \approx 18\ \mu m$. Since this is far larger than both the bacterial size and the separation of terrace steps, the bacterium will not elastically conform to the steps. This is consistent with our earlier results, where the bacterium is essentially rigid for reasonable adhesion energies.

Another possible mechanism for alignment is from small isolated edges due to step bunching or due to oxidation fronts on the pyrite surface. The interaction of the bacterium with an isolated step edge is easily found, and the geometry and the enhancement factor compared to the binding to a flat substrate is shown in Fig. 6 with respect to the step height in nm. A 20% enhancement, corresponding to a $k_B T$-binding difference with our parameters, is seen with a 10-nm step edge.

The final surface feature we will consider is a shallow pit of circular cross-section and of the approximate size of a bacterium. Fig. 7 shows the binding enhancement we would expect for a shallow cylindrical pit with the bacterial radius of curvature, as a function of depth. These calculations indicate a striking binding enhancement for all pit depths.

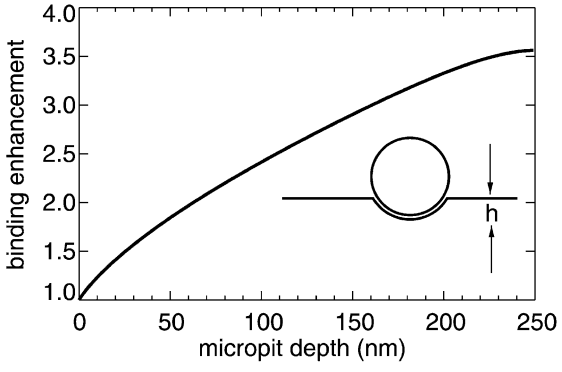

Fig. 7. The enhancement factor for a small cylindrical micropit nestling the bacterium (as shown) vs. the micropit depth, *h*. The binding strength is the enhancement factor times the binding strength on a flat substrate (see Fig. 4).

6. Experimental methods

The model system used here to examine attachment is the mineral pyrite (Wards scientific) and the sulfur-oxidizing bacterium *T. caldus* strain tc1, isolated from a sulfide ore-body site in the western United States described by Edwards et al. (1999).

6.1. Alignment experiment

Prior to experiments, strain tc1 was grown for 1 week at 37°C unshaken on elemental sulfur-based medium as described by Edwards et al. (2000a). In order to examine alignment patterns over time, 2 ml of cells were harvested by centrifugation, washed two times in distilled water that was acidified to pH 1.5 with sulfuric acid, and inoculated into a flask containing $\sim 1 \times 2 \times 2\ mm^3$ polished pyrite cubes, prepared as described elsewhere (Edwards et al., 2000a). Cells and mineral material were incubated at 37°C unshaken for 4 days. For fluorescent analysis, blocks were periodically removed from flasks with sterile forceps, and fixed in 4% paraformaldehyde in $1\times$ phosphate buffered saline solution (0.137 M NaCl, 0.005 M $NaHPO_4 * 7H_2O$, 0.003 M KCl, 0.001 M KH_2PO_4), pH 7.3, for 2 h. Fixed samples were rinsed in distilled water and air-dried. For fluorescent analysis, cells were hybridized with fluorescein-labeled bacterial probe (EUB338; Amann et al., 1995) using a whole-cell hybridization procedure described elsewhere (Edwards et al., 2000a,b). Cells were detected using a Zeiss Axiovert ST100 equipped with a Hamamatsu Orca cooled CCD video camera and Openlab software for the Macintosh computer for image capture and analysis. Supplemental image analysis software used included Adobe Photoshop and NIH image.

Cell orientations relative to {110} and {100} pyrite ($\pm 2°$, $\pm 5°$, $\pm 10°$) were analyzed using transparent overlays labeled with angular arcs. Cell orientations were analyzed for 75 fields of view ($50 \times 30\ \mu m^2$) at three sampling times over 96 h.

6.2. Time-resolved attachment experiment

In order to examine bacterial behavior at the surface prior to and during attachment, 1/2 ml of *T.*

caldus was grown as described above, harvested by centrifugation, and washed two times in distilled water acidified to pH 1.5 with sulfuric acid. Cells were then re-suspended in sulfur-free medium (above) and inoculated into one well of sterile chambered cover glass (Nalge Nunc International) that contained a polished pyrite cube (above). The activity of *T. caldus* cells was monitored for 6.5 h using reflected light differential contrast light microscopy (rDIC). During this time, a series of images were collected for 5 min every 1/2 h (~ 1–2 frames/s) with the CCD camera.

7. Experimental results

7.1. Alignment experiment

An example of fluorescently labeled cells adhered to pyrite after 95 h of incubation is presented in Fig. 8. The image represents merged rDIC and fluorescent images for the area shown, so that the mineral topography and cell attachment sites may be compared. *T. caldus* cells are red and elongate, and the

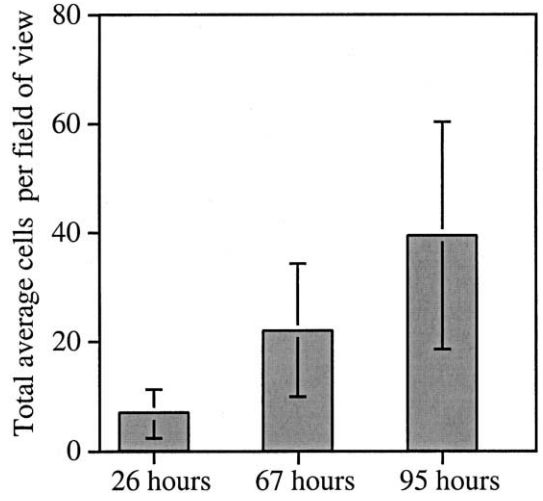

Fig. 9. Total average cells detected per field of view (see Experimental methods) over time. Also shown are the standard deviations in cell numbers between individual fields of view. Errors are approximately 1:10 of the standard deviations, so that differences are significant. The variation in time is quite close to linear, indicating that adhesion is not being significantly mediated by discrete events such as immersion, removal, and fixation of the samples.

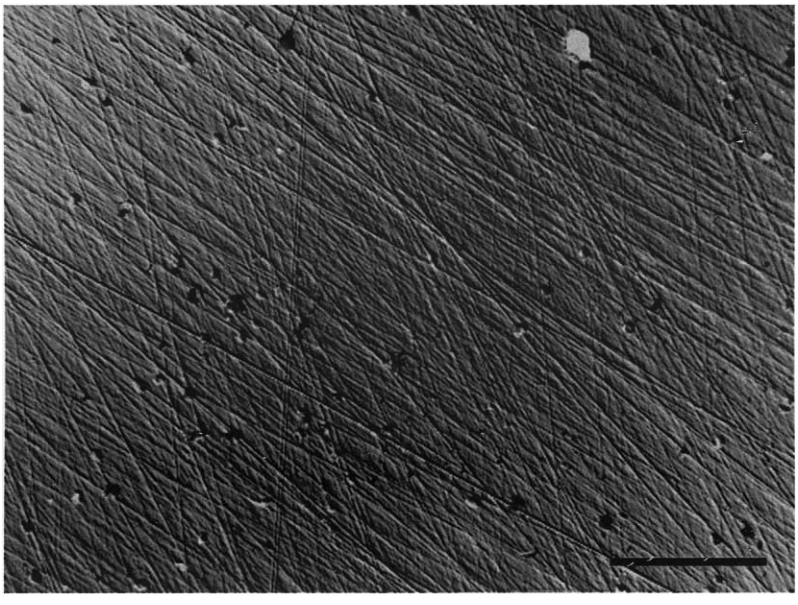

Fig. 8. An example of fluorescently labeled *T. caldus* cells adhered to a pyrite surface after 95 h of incubation. The image shows merged rDIC and fluorescent images. Cells are red and elongate (~ 0.5 × 2 μm). Scale bar is 10 μm. Cell attachment and alignment patterns seen here and observed elsewhere on all surfaces show little qualitative correspondence with the visible polishing scratches.

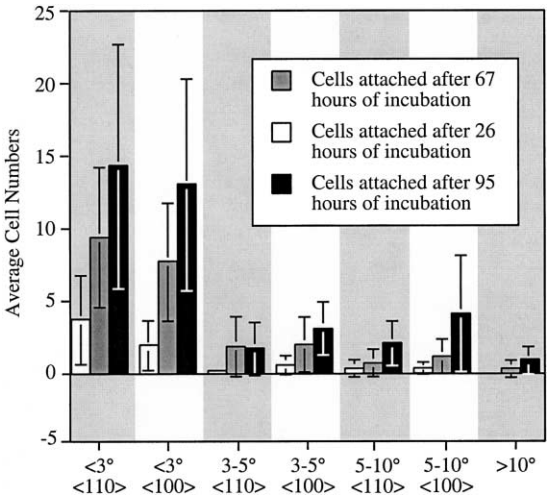

Fig. 10. Cell alignment relative to ⟨110⟩ and ⟨100⟩ pyrite over time. Average cell numbers represent data collected for 25 fields of view (see Experimental methods) per time interval. Error bars represent the standard deviation of cell populations for their specific alignment between individual fields of view.

image is oriented so that the edges are approximately parallel to [100] pyrite. As in the examples presented earlier, the adhesion localities and alignment of these cells generally show poor qualitative correspondence with the polishing scratches on the surface.

Fig. 9 presents data on cell densities detected on the surfaces over time. While average cell densities show an approximately fourfold increase from 26 to 95 h of incubation, specific cell numbers detected in each 50×30 μm^2 interval varied significantly, as reflected by the large standard deviations. Standard errors are 1/5 as large as standard deviations, so that alignment changes significantly with time.

Fig. 10 presents the cell alignment data collected from 26 to 95 h of incubation. Cell alignment data is divided into four intervals with respect to both ⟨110⟩ and ⟨100⟩ pyrite (cells aligned $\pm 2°$, 3–5°, and 5–10°, off of ⟨110⟩ and ⟨100⟩, and for $> 10°$ misalignment with respect to either). These data show that the alignment of *T. caldus* with respect to these crystallographic directions is significantly higher than misaligned attachment. No significant preferential alignment between ⟨110⟩ and ⟨100⟩ directions can be detected at any time interval.

7.2. Time-resolved attachment experiment

The series of images collected during the 6.5-h attachment experiment were compiled and converted to QuickTime movies. The complete set of QuickTime movies can be downloaded from: ftp://ftp.whoi.edu/pub/users/kedwards/caldus_movies/. After the 6.5-h period, most cells had become immobile at the surface, and were therefore presumed to be irreversibly attached. Figs. 11 and 12 are compilations of stills to show time-series data representative of the activity of *T. caldus* at the surface from the movies. Figs. 11 shows three images, taken at 0.5 (A), 1.0 (B), and 1.5 (C) h after the start of the experiment. Fig. 12 shows six images, taken at 3.5 (A, D), 4.0 (B, E), and 4.5 (C, F) h after the start of the experiment. These images are shown to illustrate

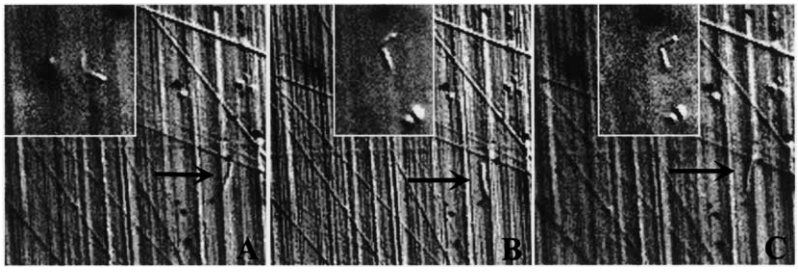

Fig. 11. Reflected-light DIC images of *T. caldus* cells at early times during the attachment experiment (see text). Frames A, B, and C were taken at 0.5, 1.0, and 1.5 h after the start of experiment, respectively. Each frame is 15 μm across. Each frame was compiled from two images taken within seconds of one another. The region outlined in white on the upper-half of the frame focuses on two cells that are ~0.5 μm from the surface. The single cell emphasized with an arrow in the lower half of the frame is very close to the focal plane of the surface. Though these cells moved while at the surface, their activity was restricted to one area of a few μm^2 near the surface.

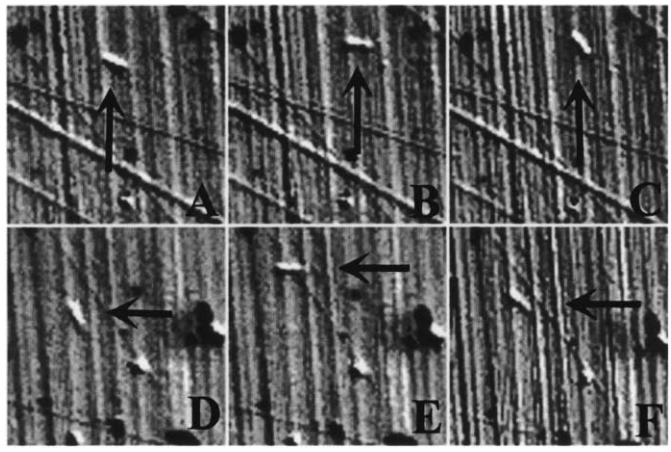

Fig. 12. Reflected-light DIC images of *T. caldus* cells at late times during the attachment experiment (see text). Frames A, B, and C were taken at 3.5, 4.0, and 4.5 h after the start of experiment, respectively. D, E, and F correspond to a different region of the same surface at the same time intervals as A, B, and C represent, respectively. Each frame is ~ 10 μm across. The same cell is tracked with an arrow in each frame. Though these cells continued to move while at the surface, it can be seen here that their activity was restricted to a small area near the surface (within a few μm^2).

that though *T. caldus* is a motile bacterium, as shown previously (Hallberg and Lindström, 1994) and observed here, prior to attachment, the activity of *T. caldus* at the surface was generally restricted to a very small area in close proximity to the surface. As exemplified in Figs. 11 and 12, we found it common for *T. caldus* cells to reside in a localized area (~ 10 μm^2) within the depth of field, in close proximity of the surface (< 0.5 μm), for a 1–3 interaction period. After 1–3 h, cells were observed to either irreversibly attach (become immobilized), or move to another area entirely.

8. Discussion

Our studies have found that (1) microtopography can significantly alter binding strength, particularly when the size and shape of the topography closely matches that of the bacterium. Hence, we would predict that topography could induce strong bias to attachment specificity. (2) There exists a strong bias for bacterial alignment parallel to principal crystallographic axis of pyrite, and little or no bias for alignment with most polishing scratches on these surfaces. (3) *T. caldus* remains in localized close proximity to the surface for considerable periods of time prior to irreversible attachment.

8.1. Dynamic interactions between metabolically active bacterial cells and dissolving minerals

Our findings suggest that we should consider how the bacterial metabolism could directly affect the mineral microtopography in situ, and what affect that would have on adhesion. *T. caldus* metabolizes secondary sulfur deposits that form on pyrite surfaces during surface growth (Edwards et al., 2000a), but does not facilitate enhanced leaching of the underlying pyrite (Hallberg and Lindström, 1994; McGuire et al., in press). Though the removal rate of sulfur has not been determined for *T. caldus*, McGuire et al. (2001) found by comparing *T. caldus* reacted samples with abiotically reacted samples that *T. caldus* apparently removes or prevents the formation of what would constitute thousands of elemental sulfur monolayers on sulfide mineral surfaces—assuming homogeneous distribution of the sulfur product. If removal is localized due to heterogeneous production of oxidants by a metabolizing bacteria in proximity of a surface (where the degree of local interaction would depend on the specific interaction

region and the diffusion rate of oxidants away from the source), then we would expect a resulting local alteration of mineral microtopography.

Though the rate of sulfur removal per cell is not known, we can make an illustrative comparison based on what has been measured for iron oxidizers; the pyrite leach rate per cell at 42°C has been estimated at 4×10^{-13} M Fe/cell/day (Edwards et al., 1998). If we estimate that 25% of the iron oxidized is converted in the vicinity of the cell/mineral interface, then we expect a leach rate of ≈ 10 nm/h over a cell area of 10 μm^2. Thus, over time periods consistent with the observed "interaction periods" for *T. caldus* at the pyrite surface (1–3 h), significant localized etching could take place with comparable rates. The formation of shallow etch pits beneath adhering bacteria is difficult to check, since bacterial-shaped pits can be similar to those produced by abiological attack (Edwards et al., 2001). Moreover, reversible detachment of bacteria and the diffusion of attached bacteria along the mineral surface can result in etch pits that are not necessarily associated with the bacteria that formed them. Additionally, the average residence time for bacteria (S- or Fe-oxidizing) reversibly attached at one place on the surface is not known. There are, however, examples that strongly suggest that local alteration of mineral microtopography due to metabolism has occurred. Fig. 13 shows a dehydrated *T. caldus* cell on a pyrite surface imaged by SEM. The light material on this surface is presumed to be amorphous or microcrystalline sulfur that is known to form on pyrite (McGuire et al., in press). It can be clearly seen that this cell is situated within a shallow pit in the sulfur layer. We infer that this pit formed due to metabolism of sulfur by *T. caldus*. Larger, more denuded sulfur-depleted regions have also been observed surrounding attached *T. caldus* cells (Edwards, unpublished data). It is important to note, however, that what we can visualize by SEM may not represent all of the sulfur that may have been there prior to analysis. It is known that the electron beam can alter surface sulfur products, often vaporizing them within minutes of exposure (Mycroft et al., 1990). Therefore, in Fig. 13 (any all other SEM data), what is imaged is what remains after exposure to the electron beam, and not necessarily all of what was originally there.

Fig. 13. *T. caldus* cells adhering to a pyrite ⟨100⟩ surface. Scale bar is 1 μm. Cells can be seen within what is interpreted to be a sulfur-leached zone, as evidenced by the precipitate-absent regions (shown with arrows) surrounding most of the cells. The *T. caldus* cells oxidize elemental sulfur that accumulates on sulfide surfaces during oxidative dissolution (McGuire et al., 2001). Figure modified after Edwards et al. (2000a).

As indicated by the calculations shown in Fig. 7, bacterial-shaped depressions can significantly affect the bacterial binding strength; depressions of only 10-nm depth can lead to a noticeable binding difference for the bacterium, one $k_B T$ for our model potential. This is a mechanism for significantly enhancing bacterial adhesion and localization. Over a time scale of approximately 1 h, dynamic interactions between a metabolizing bacterium and a dissolving mineral surface could strongly affect binding adhesion.

8.2. Localized, crystallographically controlled mineral dissolution as an alignment mechanism

From this study, we know that cells interact with the surface in a very localized area for considerable periods of time (Figs. 11 and 12). We also know that once cells are attached, they can be detected within shallow pits or zones denuded with respect to sulfur precipitates, and that these pit edges, when well

developed as shown in Fig. 13, are observed to occur parallel to principal crystallographic directions of the underlying pyrite. What we do not know from this study is when the pits/denuded regions formed—prior to or after attachment—because their formation cannot be monitored directly at the resolution of a light microscope. However, as discussed above, it is possible that localized dissolution would occur prior to attachment during the observed interaction period. If sulfur removal occurs in a crystallographically controlled manner, as it qualitatively appears to from etch-pit alignment (Fig. 13), then since adhesion energies can be significantly enhanced within even quite shallow pits (Fig. 7), a preferential alignment of cells within crystallographically aligned dissolution pits could result—as observed.

An interesting open question is what mechanism localizes the bacterium to a small area for hours, even at distances hundreds of nanometers from the substrate—much further than directly measured interaction distances of comparable bacteria—while still allowing bacterial motion. Two possibilities seem reasonable. First is initial attachment through a bacterial appendage such as a flagellum, pili, extracellular matrix, etc. (see Hermansson, 1999), and the second is chemotactic behavior of the unattached bacterium (see Edwards et al., 2000a). Both of these seem reasonable and may in fact operate in tandem, but neither effect would directly produce anisotropic binding of the bacterial body directly to the substrate—as is observed.

9. Conclusions

This study addresses a key issue of cell attachment—the relative importance of microtopography in localizing and aligning bacterial cells on mineral surfaces. While we have used relatively simple polished surfaces to study the effects of microtopographical variations, these findings are relevant to many of the variations one would expect to encounter in natural systems. In particular, we find that the shape, more than size, of a microtopographic feature is the key to total binding adhesion energy. This suggests that the ability of metabolizing cells to alter surface chemistry over very narrow regions, comparable to the area of a cell, at nanometer depths may be a stronger force for localizing and orienting cell attachment than larger, more readily observed surface features.

To make quantitative contact between these calculations and experiment, the particular interaction parameters as applied to a bacterium and its substrate, in this case *T. caldus* on pyrite, need to be determined. This can be done through direct measurement of the adhesion energy of individual bacteria, and of their force curve as a function of separation (e.g., Lower et al., 2000, 2001; Ong et al., 1999). The change of adhesion strength due to visible microtopographic features can then be quantitatively predicted and compared with direct measurements. To explore the possibility that the substrate microtopography and the bacterial alignment co-evolve through bacterial metabolism, nanometers resolution AFM studies are needed to investigate the microtopography around adhering bacteria, and to track individual bacterial orientations over long intervals.

In principle, enhanced interactions due to surface microtopography may be included as effective "structural energy" terms in a DLVO treatment. This could be useful to describe bulk bacterial attachment densities. It is clear from this study that (1) such a structural energy term will be time-dependent and will depend sensitively on surface preparation and biotic and abiotic conditions, (2) such a term would depend on the size and shape of the adhering particle, (3) such a term would have to depend on bacterial orientation to recover the alignment effects described in this paper.

Acknowledgements

We thank D. Rancourt, S. Lower and M. Jericho for the discussions and assistance. B. Hess is thanked for his continued assistance with sample preparation. Financial support was provided by the National Science Foundation (EAR-0073998 to KJE) and by the Canadian Institute of Advanced Research Program in the Science of Soft Surfaces and Interfaces (to ADR).

References

Absolom, D.R. et al., 1983. Surface thermodynamics of bacterial adhesion. Appl. Environ. Microbiol. 46, 90–97.

Amann, R.I., Ludwig, W., Schleifer, K.-H., 1995. Phylogenetic identification and in situ detection of individual microbial cells without cultivation. Microbiol. Rev. 59, 143–169.

Banfield, J.F., Hamers, R.J., 1996. Processes at minerals and surfaces with relevance to microorganisms and prebiotic synthesis. In: Banfield, J.F., Nealson, K.H. (Eds.), Geomicrobiology: Interactions Between Microbes and Minerals. Reviews in Mineralogy. Mineralogical Society of America, Washington, DC, pp. 81–122.

Bennett, P.C., Hiebert, F.K., 1992. Microbial mediation of silicate diagenesis in organic-rich natural waters. In: Kharaka, Y.K., Maest, A.S. (Eds.), Water–Rock Interaction. AA Balkema, Rotterdam, pp. 267–270.

Bennett, P.C., Hiebert, F.K., Choi, W.J., 1996. Microbial colonization and weathering of silicates in a petroleum-contaminated aquifer. Chem. Geol. 132, 45–53.

Beveridge, T.J., 1988. The bacterial surface: general considerations towards design and function. Can. J. Microbiol. 34, 363–372.

Beveridge, T.J., 1999. Structures of gram-negative cell walls and their derived membrane vesicles. J. Bacteriol. 181, 4725–4733.

Boal, D.H., 1997. Mechanical properties of the cellular cytoskeleton. Phys. Can. 53, 228–236, Sept./Oct.

Devasia, P., Natarajan, K.A., Sathyanarayana, D.N., Rao, G.R., 1993. Surface chemistry of *Thiobacillus ferrooxidans* relevant to adhesion on mineral surfaces. Appl. Environ. Microbiol. 59, 4051–4055.

Edwards, K.J., Schrenk, M.O., Hamers, R., Banfield, J.F., 1998. Microbial oxidation of pyrite: experiments using microorganisms from an extreme acidic environment. Am. Mineral. 83, 1444–11453.

Edwards, K.J. et al., 1999. Geomicrobiology of pyrite (FeS_2) dissolution: a case study at Iron Mountain, California. Geomicrobiol. J. 16 (2), 155–179.

Edwards, K.J., Bond, P.L., Banfield, J.F., 2000a. Characteristics of attachment and growth of *Thiobacillus caldus* on sulfide minerals: a chemotactic response to sulfur minerals? Environ. Microbiol. 2, 324–332.

Edwards, K.J., Bond, P.L., Gihring, T.M., Banfield, J.F., 2000b. An Archaeal iron-oxidizing extreme acidophile important in acid mine drainage. Science 279, 1796–1799.

Edwards, K.J., Hu, B., Hamers, R.J., Banfield, J.F., 2001. A new look at microbial leaching patterns on sulfide minerals. FEMS Microbiol. Ecol. 34, 197–206.

Eggleston, C.M., 1997. Initial oxidation of sulfide sites on a galena surface; experimental confirmation of an ab initio calculation. Geochim. Cosmochim. Acta 61 (3), 657–660.

Eggleston, C.M., Ehrhardt, J.J., Stumm, W., 1996. Surface structural controls on pyrite oxidation kinetics; an XPS-UPS, STM, and modeling study. Am. Mineral. 81 (9–10), 1036–1056.

Hallberg, K.B., Lindström, E.B., 1994. Characterization of *Thiobacillus caldus* sp. nov., a moderately thermophilic acidophile. Microbiology 140, 3451–3456.

Hazen, T.C., JimJimenez, L., de Vectoria, G.L., 1991. Comparison of bacteria from the deep subsurface sediment and adjacent groundwater. Microb. Ecol. 22, 293–304.

Hermansson, M., 1999. The DLVO theory in microbial adhesion. Colloids Surf. B 14, 105–119.

Hiebert, F.K., Bennett, P.C., 1992. Microbial control of silicate weathering in organic-rich ground water. Science 258, 278–281.

Landau, L.D., Lifshitz, E.M., 1986. Theory of Elasticity. 3rd edn. Pergamon, New York.

Lower, S.K., Tadanier, C.J., Hochella Jr., M.F., 2000. Measuring interfacial and adhesion forces between bacteria and mineral surfaces with biological force microscopy. Geochim. Cosmochim. Acta 64, 3133–3139.

Lower, S.K., Hochella Jr., M.F., Beveridge, T.J., 2001. Bacterial recognition of mineral surfaces: nanoscale interactions between *Shewanella* and α-FeOOH. Science 292, 1360–1363.

Marshall, K.C., Stout, R., Mitchell, R., 1971. Mechanism of the initial events in the sorption of marine bacteria to surfaces. J. Gen. Microbiol. 68, 337–348.

McGuire, M.M., Edwards, K.J., Banfield, J.F., Hamers, R.J., 2001. Kinetics, surface chemistry, and structural evolution of microbially mediated sulfide mineral dissolution. Geochim. Cosmochim. Acta. 65, 1243–1258.

Meinders, J.M., van der Mei, H.C., Busscher, H.J., 1995. Deposition efficiency and reversibility of bacterial adhesion under flow. J. Colloid Interface Sci. 176, 329–341.

Morisaki, H., 1991. Measurement of the force necessary for removal of bacterial cells from a quartz plate. J. Gen. Microbiol. 137, 2649–2655.

Mycroft, J.R., Bancroft, G.M., McIntyre, N.S., Lorimer, J.W., Hill, I.R., 1990. Detection of sulphur and polysulfides on electrochemically oxidized pyrite surfaces by X-ray photoelectron spectroscopy and Raman spectroscopy. J. Electroanal. Chem. 292, 139–152.

Ong, Y.-L., Razatos, A., Georgiou, G., Sharma, M.M., 1999. Adhesion forces between *E. coli* bacteria and biomaterial surfaces. Langmuir 15, 2719–2725.

Overmann, J., Lehmann, S., Pfennig, N., 1991. Gas vesicle formation and buoyancy regulation in *Pelodictyon phaeoclathratiforme* (green sulfur bacteria). Arch. Microbiol. 157, 29–37.

Pinette, M.F.S., Koch, A.L., 1987. Variability of the turgor pressure of individual cells of the gram-negative heterotroph *Ancylobacter aquaticus*. J. Bacteriol. 169, 4742–4747.

Scholl, M.A., Mills, A.L., Herman, J.S., Hornberger, G.M., 1990a. The influence of mineralogy and solution chemistry on the attachment of bacteria to representative aquifer material. J. Contam. Hydrol. 6, 321–326.

Scholl, M.A., Mills, A.L., Herman, J.S., Hornberger, G.M., 1990b. The influence of mineralogy and solution chemistry on the attachment of bacteria to representative aquifer materials. J. Contam. Hydrol. 6, 321–336.

Silverman, M.P., Ehrlich, H.L., 1964. Microbial formation and degradation of minerals. Adv. Appl. Microbiol. 6, 153–206.

Swain, P.S., Andelman, D., 1999. The influence of substrate structure on membrane adhesion. Langmuir 15, 8902–8914.

Thwaites, J.J., Surana, U.C., 1991. Mechanical properties of *Bacillus subtilis* cell walls: effects of removing residual culture medium. J. Bacteriol. 173, 197–203.

van Loosdrecht, M.C., Lyklema, J., Norde, W., Zehnder, A.J., 1989. Bacterial adhesion: a physicochemical approach. Microb. Ecol. 17, 1–15.

van Loosdrecht, M.C.M., Lyklema, J., Norde, W., Zehnder, A.J.B.,

1990a. Influence of interfaces on microbial activity. Microbiol. Rev. 54 (1), 75–87.

van Loosdrecht, M.C.M., Norde, W., Lyklema, J., Zehnder, A.J.B., 1990b. Hydrophobic and electrostatic parameters in bacterial adhesion. Aquat. Sci. 52 (1), 103–114.

Yao, X., Jericho, M., Pink, D., Beveridge, T., 1999. Thickness and elasticity of gram-negative murein sacculi measured by atomic force microscopy. J. Bacteriol. 181, 6865–6875.

Yee, N., Fein, J.B., Daughney, C.J., 1999. Experimental study of the pH, ionic strength, and reversibility behavior of bacteria–mineral adsorption. Geochim. Cosmochim. Acta 64, 609–617.